

¹⁸F-FDG Accumulation in Atherosclerotic Plaques: Immunohistochemical and PET Imaging Study

Mikako Ogawa, MS^{1,2}; Seigo Ishino, BS³; Takahiro Mukai, PhD⁴; Daigo Asano, BS³; Noboru Teramoto, BS¹; Hiroshi Watabe, PhD¹; Nobuyuki Kudomi, PhD¹; Masashi Shiomi, PhD⁵; Yasuhiro Magata, PhD²; Hidehiro Iida, PhD¹; and Hideo Saji, PhD³

¹Department of Investigative Radiology, Research Institute, National Cardiovascular Center, Suita, Japan; ²Laboratory of Genome Bio-Photonics, Photon Medical Research Center, Hamamatsu University School of Medicine, Hamamatsu, Japan; ³Department of Pathofunctional Bioanalysis, Graduate School of Pharmaceutical Sciences, Kyoto University, Kyoto, Japan; ⁴Department of Nuclear Medicine and Diagnostic Imaging, Graduate School of Medicine, Kyoto University, Kyoto, Japan; and ⁵Institute for Experimental Animals, Kobe University School of Medicine, Kobe, Japan

The rupture of atherosclerotic plaques and the subsequent formation of thrombi are the main factors responsible for myocardial and cerebral infarctions. Thus, the detection of vulnerable plaques in atherosclerotic lesions is a desirable goal, and attempts to image these plaques with ¹⁸F-FDG have been made. In the present study, the relationship between the accumulation of ¹⁸F-FDG and the biologic characteristics of atherosclerotic lesions was investigated. Furthermore, PET imaging of vulnerable plaques was performed with an animal model of atherosclerosis, Watanabe heritable hyperlipidemic (WHHL) rabbits. **Methods:** WHHL ($n = 11$) and control ($n = 3$) rabbits were injected intravenously with ¹⁸F-FDG, and the thoracic and abdominal aortas were removed 4 h after injection. The accumulated radioactivity was measured, and the number of macrophages and the intimal area were investigated by examination of stained sections. PET and CT images were also acquired at 210 min after injection of the radiotracer. **Results:** ¹⁸F-FDG accumulated to a significantly higher level in the aortas of the WHHL rabbits (mean \pm SD differential uptake ratio [DUR], 1.47 ± 0.90) than in those of the control rabbits (DUR, 0.44 ± 0.15); DUR was calculated as (tissue activity/tissue weight)/(injected radiotracer activity/animal body weight), with activities given in becquerels and weights given in kilograms. ¹⁸F-FDG uptake and the number of macrophages were strongly correlated in the atherosclerotic lesions of the WHHL rabbits ($R = 0.81$). In the PET analysis, intense ¹⁸F-FDG radioactivity was detected in the aortas of the WHHL rabbits, whereas little radioactivity was seen in the control rabbits. **Conclusion:** The results suggest that macrophages are responsible for the accumulation of ¹⁸F-FDG in atherosclerotic lesions. Because vulnerable plaques are rich in macrophages, ¹⁸F-FDG imaging should be useful for the selective detection of such plaques.

Key Words: ¹⁸F-FDG; atherosclerosis; vulnerable plaque; macrophage; Watanabe heritable hyperlipidemic rabbit

J Nucl Med 2004; 45:1245–1250

The disruption of atherosclerotic plaques and the subsequent formation of thrombi are currently recognized as the primary mechanisms of myocardial and cerebral infarctions (1). Atherosclerotic plaques are classified into 2 types, stable and vulnerable, the latter having a high risk of rupture. Thus, the detection of vulnerable plaques is clinically important for risk stratification and to provide early treatment.

Plaque vulnerability is characterized by a large lipid-rich atheromatous core, a thin fibrous cap, and infiltration by inflammatory cells, such as macrophages (2–5). Several imaging approaches have been adapted to detect vulnerable atherosclerotic plaques (6). Conventional x-ray contrast angiography detects morphologic characteristics, such as stenosis. However, because both types of plaques cause stenosis (7), it is difficult to determine whether a plaque is stable or vulnerable by x-ray contrast angiography. MRI approaches, including magnetic resonance angiography, have also been developed by use of gradient-echo techniques and have been successful in discriminating lipid cores, fibrous caps, and hemorrhaged lesions (8,9). Moreover, an intravascular ultrasonography technique that can directly image an atheroma recently was reported (10). These new approaches provide images based on the morphologic characteristics of the atheroma but do not provide biologic information, such as the presence of inflammation, which is an important characteristic of vulnerable plaque.

Meanwhile, nuclear medical techniques are able to detect atherosclerotic lesions along with biopathologic functions and therefore offer a great advantage for the discrimination of vulnerable plaques on the basis of biologic characteristics (11). In fact, a clinical trial to detect atherosclerotic lesions by nuclear medical imaging with ¹⁸F-FDG recently was reported (12). However, there is the possibility that ¹⁸F-FDG is taken up by surrounding cells, including smooth muscle cells, as well as macrophages that have infiltrated vulnerable plaques, because glucose is an essential substrate

Received Sep. 8, 2003; revision accepted Mar. 12, 2004.
For correspondence or reprints contact: Hideo Saji, PhD, Department of Pathofunctional Bioanalysis, Graduate School of Pharmaceutical Sciences, Kyoto University, Sakyo-ku, Kyoto 606-8501, Japan.
E-mail: hsaji@pharm.kyoto-u.ac.jp

for energy production in various cells. The uptake of radioactivity by the tissue surrounding vulnerable plaques, including the blood, prevents the visualization of the plaques. Thus, to evaluate the usefulness of ^{18}F -FDG for imaging vulnerable plaques, it is necessary to clarify causative biologic factors in the uptake of ^{18}F -FDG by atherosclerotic lesions.

Watanabe heritable hyperlipidemic (WHHL) rabbits have been widely used as an animal model of atherosclerosis (13,14). In WHHL rabbits, the atherosclerotic plaque does not rupture, but its pathologic characteristics have been reported to resemble those of the human lesion (15,16,17). Thus, although the aortic plaque of WHHL rabbits does not reflect the plaque rupture process absolutely, the use of aortic segments of WHHL rabbits could be effective for investigating the biologic factors responsible for the accumulation of ^{18}F -FDG.

Therefore, in the present study, by using the WHHL rabbit aorta, we investigated the relationship between the accumulation of ^{18}F -FDG and the biopathologic characteristics of atherosclerotic lesions (macrophage density and intimal thickness) and performed PET imaging of vulnerable plaques.

MATERIALS AND METHODS

Animals

Eleven WHHL rabbits (12–29 mo old) bred at Kobe University and weighing 2.9–3.6 kg were used in the present study. The animals were fed standard rabbit chow (type CR-3; Clea Japan Inc.) at 120 g/d and were given water ad libitum. For the control study, 3 New Zealand White rabbits (3–8 mo old; Kitayama Labs) weighing 3.0–3.2 kg were used. The animals were fasted for at least 4 h before receiving ^{18}F -FDG. All experiments were approved by the Animal Care and Use Committee of the National Cardiovascular Center.

^{18}F -FDG Distribution

The rabbits were initially anesthetized with a bolus injection of sodium pentobarbital (30 mg/kg, intravenous), followed by a continuous injection of propofol (10 mg/kg/h, intravenous). ^{18}F -FDG (260–555 MBq) was injected into a marginal ear vein. Arterial blood samples were collected from an auricular artery at 60, 120, 180, and 240 min after injection of the radiotracer. At 4 h after the ^{18}F -FDG injection, the animals were sacrificed with an overdose of sodium pentobarbital. The thoracic and abdominal aortas were removed, and adjacent fat and connective tissue were detached. The aortas were cut into 6-mm segments and weighed. The segments were immediately fixed in a solution containing L-(+)-lysine hydrochloride (75 mmol/L) and 4% paraformaldehyde in phosphate buffer (37.5 mmol/L; pH 7.4), and radioactivity was measured with a well-type γ -counter (PS-201; Aloka Co., Ltd.). Blood samples were also weighed, and radioactivity was measured. The results were expressed as the differential uptake ratio (DUR), which was calculated as (tissue activity/tissue weight)/(injected radiotracer activity/animal body weight), with activities given in becquerels and weights given in kilograms.

Histologic Analysis

Each arterial segment was embedded in paraffin. Consecutive 5- μm -thick slices were prepared 1, 3, and 5 mm from the end of the 6-mm segments used to measure radioactivity. The slices were subjected to Azan-Mallory staining or immunohistochemical staining. Immunohistochemical analysis was performed by the method of Tsukada et al. (18) with rabbit macrophage-specific monoclonal antibody RAM-11 (Dako Corp.). These slices were also costained with hematoxylin for identification of the nucleus. The number of macrophages was determined by counting the nuclei of RAM-11-positive cells in each slice. The Azan-Mallory-stained slice image was read with an optical scanner, and the intimal and whole areas of the vessels were measured. The density of macrophages and the ratio of the area of the intima to the area of the whole cross section in each 6-mm segment were obtained by averaging the data at the 3 positions, 1, 3, and 5 mm. The data for each 6-mm segment were used for comparison with ^{18}F -FDG uptake.

CT and PET Imaging

CT and ^{18}F -FDG PET experiments were performed on each normal and WHHL rabbit before sacrifice. The rabbits were fixed on a board and moved carefully from a CT scanner (Auklet TSX-003A; Toshiba Co., Ltd.) to a PET scanner (ECAT EXACT HR; Siemens AG) to maintain the stereotactic position on the board. Iohexol, a contrast agent, was injected through a marginal ear vein. A helical CT angiogram was acquired at 180 min after injection of ^{18}F -FDG, and PET scanning was performed for 15 min starting at 210 min after injection of ^{18}F -FDG. PET images and CT images were automatically coregistered by use of automatic image registration software (19). PET images were calibrated to the injected dose of ^{18}F -FDG. For measurement of radioactivity in the thoracic aorta, 6 circular regions of interest (4.1 mm² for each region of interest) were drawn on the successive cross sections (1 mm apart) of the aorta.

Statistical Analysis

Data are presented as the mean \pm SD. Statistical analysis was performed with the Mann-Whitney U test for comparing the aortic segments of the control and WHHL rabbits. Correlation coefficients were assessed with Spearman rank correlation coefficients. Statistical significance was established at a *P* value of <0.05.

RESULTS

^{18}F -FDG Distribution

The DURs in the aortic segments and the aortic tissue-to-blood radioactivity ratios for the normal and WHHL rabbits at 4 h after injection of ^{18}F -FDG are summarized in Table 1. ^{18}F -FDG was taken up to a significantly greater extent in the aortas of the WHHL rabbits than in those of the control rabbits. In the WHHL rabbits, higher levels of radioactivity were observed in the thoracic aorta than in the abdominal aorta, whereas only a slight difference was seen in the control rabbits. The time-activity curves for the blood were similar in all of the rabbits studied. The aortic tissue-to-blood radioactivity ratios were significantly higher in the WHHL rabbits than in the control rabbits.

Histologic Analysis

Typical images of the Azan-Mallory-stained and immunohistochemically stained slices are shown in Figure 1. The

TABLE 1
Accumulation of ^{18}F -FDG in Aortic Segments and Number of Macrophages

Parameter	Mean \pm SD for indicated portion of aorta in following rabbits*:			
	Control ($n = 3$)		WHHL ($n = 11$)	
	Abdominal	Thoracic	Abdominal	Thoracic
^{18}F -FDG uptake (DUR)	0.40 ± 0.11	0.44 ± 0.15	$0.72 \pm 0.37^\dagger$	$1.47 \pm 0.90^\ddagger$
Aortic segment-to-blood radioactivity ratio	1.06 ± 0.35	1.23 ± 0.34	$1.77 \pm 0.86^\S$	$3.18 \pm 1.19^\ddagger$
No. of macrophages	ND	ND	254 ± 257	737 ± 486

*Determined at 4 h after injection of ^{18}F -FDG.

$^\dagger P < 0.01$ vs. control group.

$^\ddagger P < 0.0001$ vs. control group.

$^\S P < 0.005$ vs. control group.

ND = not detected.

intima was scarcely perceivable in the control rabbits, whereas the intimal thickness was marked in the WHHL rabbits. Macrophages were found in the intimal lesions of most WHHL rabbits, and the extent of their infiltration was greater in the thoracic aorta than in the abdominal aorta in all WHHL rabbits (Table 1). Furthermore, there was no correlation between macrophage number and the ratio of the area of the intima to the area of the whole cross section. No macrophages were seen in the aortas of the control rabbits.

Correlation Between ^{18}F -FDG Uptake and Histologic Findings

^{18}F -FDG accumulation and the number of macrophages in the atherosclerotic lesions were well correlated ($R = 0.81$, $P < 0.0001$) (Fig. 2A). On the other hand, the correlation between ^{18}F -FDG uptake and the ratio of the area of

the intima to the area of the whole cross section was poor ($R = 0.34$) (Fig. 2B).

CT and PET Imaging

Figure 3 shows the CT images, PET images, and superimposed PET/CT images for the control and WHHL rabbits. The aortas could not be imaged in the control rabbits (Fig. 3F). In contrast, intense radioactivity was observed in the WHHL rabbit aortas (Fig. 3C). The measured radioactivities in the WHHL rabbit thoracic aortas and control rabbit thoracic aortas on the PET images were 72.50 ± 9.39 and 12.90 ± 0.28 kBq/mL, respectively; the value in the WHHL rabbits was significantly higher than that in the control rabbits ($P < 0.001$). The radioactivities in the thoracic aortic segments removed from the WHHL and control rabbits, as measured with a well-type γ -counter, were $209.3 \pm$

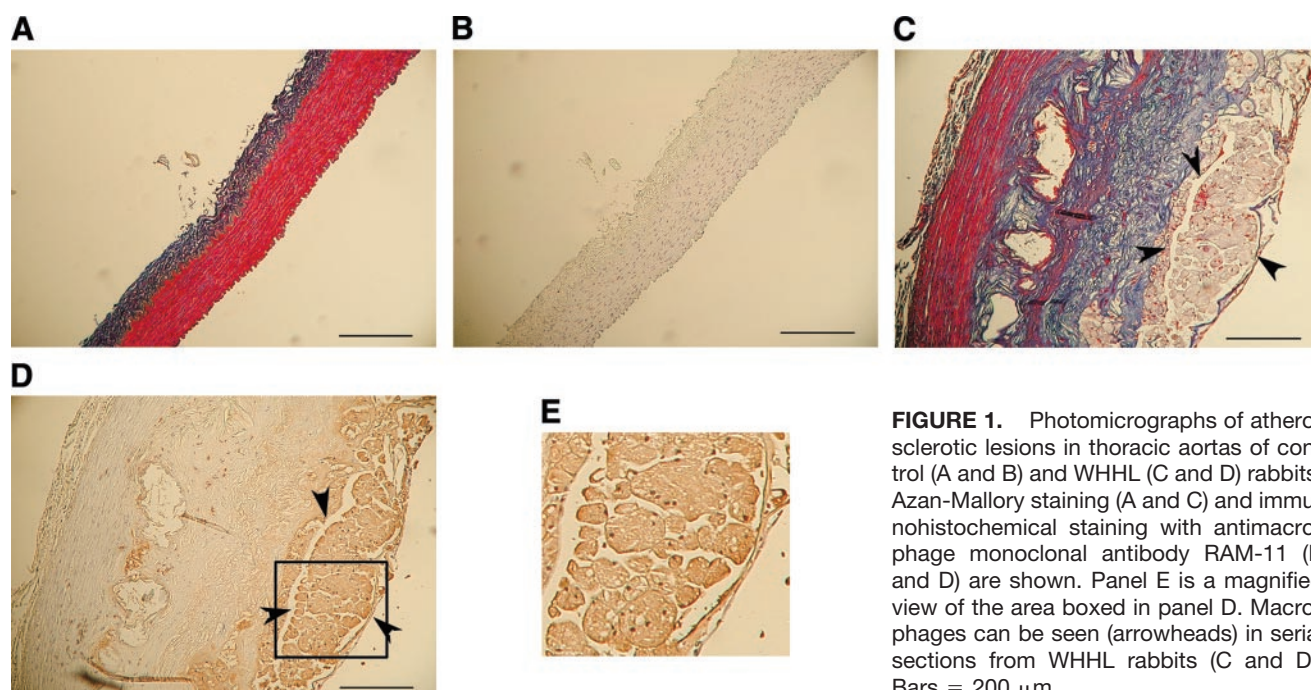
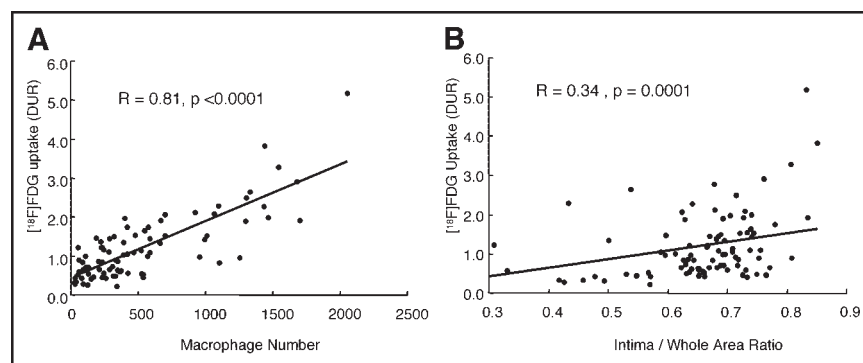


FIGURE 1. Photomicrographs of atherosclerotic lesions in thoracic aortas of control (A and B) and WHHL (C and D) rabbits. Azan-Mallory staining (A and C) and immunohistochemical staining with antimacrophage monoclonal antibody RAM-11 (B and D) are shown. Panel E is a magnified view of the area boxed in panel D. Macrophages can be seen (arrowheads) in serial sections from WHHL rabbits (C and D). Bars = 200 μm .

FIGURE 2. Correlation between ^{18}F -FDG uptake and macrophage number in aortic segments ($n = 86$) (A) or between ^{18}F -FDG uptake and the ratio of the area of the intima to the area of the whole cross section in aortic segments ($n = 86$) (B) from WHHL rabbits.



34.2 and 184.3 ± 17.0 kBq/g, respectively, and the DURs corrected for the body weight and the injected dose were 1.03 ± 0.16 and 0.71 ± 0.07 , respectively; the DUR in the WHHL rabbits was significantly higher than that in the control rabbits ($P < 0.05$).

DISCUSSION

In the present study, we investigated the relationship between the accumulation of ^{18}F -FDG and the pathologic characteristics of aortic atherosclerotic lesions in WHHL rabbits.

In the aortas of the control rabbits, the intima was thin, and no macrophages were seen. However, in those of the WHHL rabbits, a thick intima and macrophage infiltration were observed. These pathologic findings in the WHHL rabbits are consistent with results reported previously (16,20).

The uptake of ^{18}F -FDG in the WHHL rabbits was studied comparatively by using a control group. As shown in Table 1, uptake was significantly higher in the aortas of the WHHL rabbits than in those of the control rabbits. Furthermore, in the WHHL rabbits, higher ^{18}F -FDG accumulation was observed in the thoracic aorta than in the abdominal aorta. Because macrophage density was greater in the thoracic aorta than in the abdominal aorta, the increased ^{18}F -FDG accumulation in the thoracic aorta may have been attributable to the macrophage density (Table 1). Therefore,

in the WHHL rabbits, the relationship between the accumulation of ^{18}F -FDG and the biopathologic characteristics of the atherosclerotic lesions, including the number of macrophages, was quantitatively examined.

In general, the intima is inflamed and extensive macrophage infiltration is observed in vulnerable plaques. In contrast, in stable plaques, the intima is not inflamed and macrophages have not infiltrated (2–5). Therefore, the relationship between ^{18}F -FDG accumulation and the number of macrophages in atherosclerotic lesions was investigated. The accumulation of ^{18}F -FDG was well correlated with the number of macrophages (Fig. 2A). Furthermore, the relationship between ^{18}F -FDG accumulation and intimal thickness was examined. In a comparison of vulnerable plaques and stable plaques, the intimal thicknesses are similar, but the components of the intima are different; macrophage density is greater in vulnerable plaques than in stable plaques, and smooth muscle cells are the major cellular components of stable plaques (21). If cells other than macrophages, such as smooth muscle cells, contribute to accelerated ^{18}F -FDG uptake, then the accumulation of ^{18}F -FDG should be correlated with intimal thickness. However, the correlation between ^{18}F -FDG uptake and the ratio of the area of the intima to the area of the whole cross section was poor (Fig. 2B). Also, there was no relationship between the number of macrophages and intimal thickness. These findings suggest that macrophage density is mainly responsible

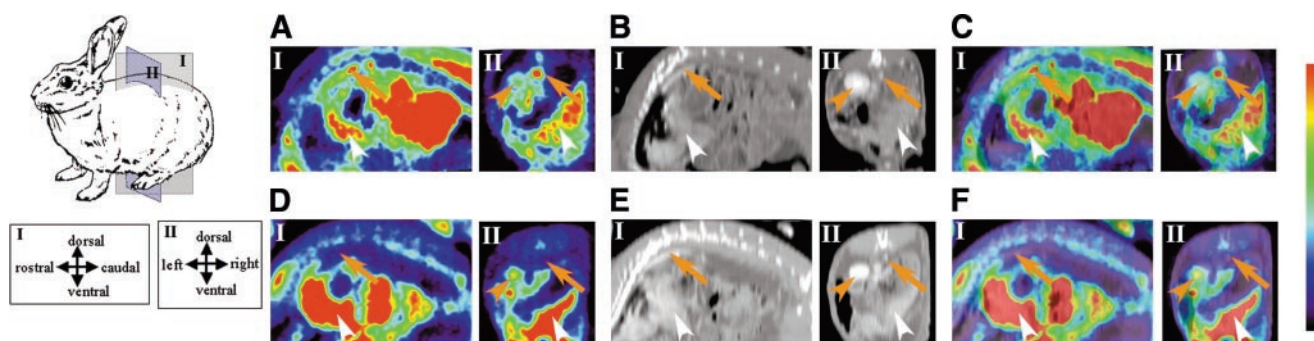


FIGURE 3. PET images (A and D), CT images (B and E), and superimposed PET/CT images (C and F) in the sagittal (I) and coronal (II) planes for WHHL (A, B, and C) and control (D, E, and F) rabbits. Orange arrows, orange arrowheads, and white arrowheads indicate aortas, kidneys, and livers, respectively.

for ^{18}F -FDG accumulation in plaques. In fact, both Rudd et al. and Lederman et al. showed that tritium-labeled glucose analogs accumulate in macrophage-rich atherosclerotic plaques in vitro (12,22). These reports are consistent with our in vivo findings.

Furthermore, it was reported that macrophages contribute extensively to the development of inflammation in plaques (23,24), and ruptured plaques have large numbers of macrophages (25). Thus, macrophage density is considered an important determinant of plaque vulnerability. Therefore, the finding that ^{18}F -FDG uptake is directly proportional to macrophage density suggests the usefulness of ^{18}F -FDG for the assessment of plaque vulnerability.

PET imaging with ^{18}F -FDG detected intense radioactivity in the WHHL rabbit aortas, whereas the control rabbit aortas could not be imaged (Fig. 3). Because the blood-to-atherosclerotic lesion ratio in the WHHL rabbits was higher than that in the control rabbits and no difference was detected in blood radioactivities between the control and the WHHL rabbits, these results indicate that the strong radioactivity detected by PET in the WHHL rabbit aortas was attributable to vulnerable plaques and not to blood. In fact, the radioactivities in both the thoracic aortic lesions measured by PET and the removed thoracic aortic segments measured by the well-type γ -counter were higher in the WHHL rabbits than in the control rabbits. However, the radioactivity measured by PET was lower than that measured by the well-type γ -counter. This underestimation could have been attributable to the low spatial resolution of the PET scanner (full width at half maximum, 6 mm). Because the diameter of the aorta is smaller than the spatial resolution, 5 mm for the WHHL rabbits and 2.5 mm for the control rabbits, a partial-volume effect can be observed. The radioactivity was underestimated more in the control rabbits because the aorta is thinner in these rabbits than in the WHHL rabbits. The radioactivity obtained by the well-type γ -counter was higher in the WHHL rabbits than in the control rabbits, but the difference was not significant. However, the DUR in the WHHL rabbits was significantly higher than that in the control rabbits because of differences in body weight and injected dose.

Because atherosclerotic plaques are small and the spatial resolution of PET is low, the use of new imaging devices will be required to image vulnerable atherosclerotic plaques accurately. Devices combining PET and CT or MRI have been developed to overcome the lack of anatomic information on PET images (26); in fact, the routine clinical use of PET/CT scanners is now under way (27). These techniques should make it possible to detect ^{18}F -FDG accumulation in vulnerable plaques in atherosclerosis. However, the detection of carotid plaques with ^{18}F -FDG PET would be difficult because the carotid artery is too narrow. The detection of coronary plaques would also be difficult because of high myocardial background radioactivity and cardiac motion. These difficulties might be overcome by use of a small positron-sensitive detector that can be inserted into the

coronary artery and placed in close contact with lesions (22,28,29).

Determination of the ^{18}F -FDG uptake for discriminating stable and vulnerable plaques is clinically important. It is applicable in assessing the risk of rupture among atherosclerotic plaques and in judging the therapeutic effect of some pharmaceutical agents for atheromas, such as statins. However, for these purposes, there is a limitation in studies with WHHL rabbits. Therefore, we did not evaluate the accuracy of ^{18}F -FDG for distinguishing vulnerable from stable plaques. In WHHL rabbits, the rupture of aortic atherosclerotic plaques was not observed; moreover, there was considerable overlap, with some segments having large numbers of macrophages but little or no increase in ^{18}F -FDG uptake, although there was a good correlation between the accumulation of ^{18}F -FDG and the number of macrophages (Fig. 2A). It has been reported that the formation of aortic atherosclerotic plaques is related to the age of WHHL rabbits (20), although that relationship was not clear from the present study. In addition, vulnerable plaques are characterized by several features, such as a thin cap, in addition to the number of macrophages. Thus, further study of the relationship between the accumulation of ^{18}F -FDG and factors such as age and cap thickness is required.

CONCLUSION

In the present study, we revealed that macrophages are responsible for the accumulation of ^{18}F -FDG in atherosclerotic lesions. Thus, because macrophages play a pivotal role in plaque rupture, ^{18}F -FDG imaging is suggested to be useful for the selective detection of vulnerable plaques. Therefore, ^{18}F -FDG PET imaging should be clinically effective for assessing the risk of plaque rupture, although there may be a limitation relating to the size and site of plaques because of the low spatial resolution of PET.

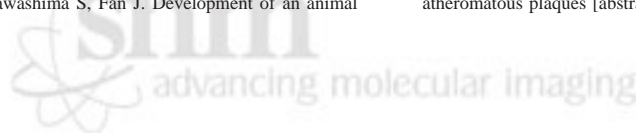
ACKNOWLEDGMENTS

This study was supported by the Program for Promotion of Fundamental Studies in Health Science of the Organization for Pharmaceutical Safety and Research of Japan and by Sankyo Foundation of Life Science. We thank Dr. Takashi Ito, Kobe University School of Medicine, and Dr. Takuga Hayashi, National Cardiovascular Center, for technical assistance and useful discussions and Norimasa Ejima, Institute for Biofunctional Research Ltd., for cyclotron operation and ^{18}F -FDG synthesis.

REFERENCES

1. Lendon C, Born GV, Davies MJ, et al. Plaque fissure: the link between atherosclerosis and thrombosis. *Nouv Rev Fr Hematol*. 1992;34:27–29.
2. Libby P, Geng YJ, Aikawa M, et al. Macrophages and atherosclerotic plaque stability. *Curr Opin Lipidol*. 1996;7:330–335.
3. Zhou J, Chew M, Ravn HB, et al. Plaque pathology and coronary thrombosis in the pathogenesis of acute coronary syndromes. *Scand J Clin Lab Invest Suppl*. 1999;230:3–11.
4. Libby P. Coronary artery injury and the biology of atherosclerosis: inflammation, thrombosis, and stabilization. *Am J Cardiol*. 2000;86:3J–8J.

5. Virmani R, Burke AP, Farb A, et al. Pathology of the unstable plaque. *Prog Cardiovasc Dis*. 2002;44:349–356.
6. Vallabhajosula S, Fuster V. Atherosclerosis: imaging techniques and the evolving role of nuclear medicine. *J Nucl Med*. 1997;38:1788–1796.
7. Libby P. Molecular bases of the acute coronary syndromes. *Circulation*. 1995; 91:2844–2850.
8. Pennell DJ, Bogren HG, Keegan J, Firmin DN, Underwood SR. Assessment of coronary artery stenosis by magnetic resonance imaging. *Heart*. 1996;75:127–133.
9. Johnstone MT, Botnar RM, Perez AS, et al. In vivo magnetic resonance imaging of experimental thrombosis in a rabbit model. *Arterioscler Thromb Vasc Biol*. 2001;21:1556–1560.
10. von Birgelen C, Slager CJ, Di Mario C, de Feyter PJ, Serruys PW. Volumetric intracoronary ultrasound: a new maximum confidence approach for the quantitative assessment of progression-regression of atherosclerosis? *Atherosclerosis*. 1995;118(suppl):S103–S113.
11. Blankenberg FG, Strauss HW. Nuclear medicine applications in molecular imaging. *J Magn Reson Imaging*. 2002;16:352–361.
12. Rudd JH, Warburton EA, Fryer TD, et al. Imaging atherosclerotic plaque inflammation with [¹⁸F]-fluorodeoxyglucose positron emission tomography. *Circulation*. 2002;105:2708–2711.
13. Watanabe Y. Serial inbreeding of rabbits with hereditary hyperlipidemia (WHHL-rabbit). *Atherosclerosis*. 1980;36:261–268.
14. Shiomi M, Ito T, Shiraishi M, et al. Inheritability of atherosclerosis and the role of lipoproteins as risk factors in the development of atherosclerosis in WHHL rabbits: risk factors related to coronary atherosclerosis are different from those related to aortic atherosclerosis. *Atherosclerosis*. 1992;96:43–52.
15. Buja LM, Kita T, Goldstein JL, Watanabe Y, Brown MS. Cellular pathology of progressive atherosclerosis in the WHHL rabbit: an animal model of familial hypercholesterolemia. *Arteriosclerosis*. 1983;3:87–101.
16. Shiomi M, Ito T, Tsukada T, Yata T, Ueda M. Cell compositions of coronary and aortic atherosclerotic lesions in WHHL rabbits differ: an immunohistochemical study. *Arterioscler Thromb*. 1994;14:931–937.
17. Shiomi M, Ito T, Yamada S, Kawashima S, Fan J. Development of an animal model for spontaneous myocardial infarction (WHHLMI rabbit). *Arterioscler Thromb Vasc Biol*. 2003;23:1239–1244.
18. Tsukada T, Rosenfeld M, Ross R, et al. Immunocytochemical analysis of cellular components in atherosclerotic lesions: use of monoclonal antibodies with the Watanabe and fat-fed rabbit. *Arteriosclerosis*. 1986;6:601–613.
19. Woods RP, Cherry SR, Mazziotta JC. Rapid automated algorithm for aligning and reslicing PET images. *J Comput Assist Tomogr*. 1992;16:620–633.
20. Ito T, Tsukada T, Ueda M, et al. Immunohistochemical and quantitative analysis of cellular and extracellular components of aortic atherosclerosis in WHHL rabbits. *J Atheroscler Thromb*. 1994;1:45–52.
21. Stary HC, Blankenhorn DH, Chandler AB, et al. A definition of the intima of human arteries and of its atherosclerosis-prone regions: a report from the Committee on Vascular Lesions of the Council on Arteriosclerosis, American Heart Association. *Arterioscler Thromb*. 1992;12:120–134.
22. Lederman RJ, Raylman RR, Fisher SJ, et al. Detection of atherosclerosis using a novel positron-sensitive probe and 18-fluorodeoxyglucose (FDG). *Nucl Med Commun*. 2001;22:747–753.
23. Robbie L, Libby P. Inflammation and atherothrombosis. *Ann N Y Acad Sci*. 2001;947:167–179.
24. Libby P. Inflammation in atherosclerosis. *Nature*. 2002;420:868–874.
25. van der Wal AC, Becker AE, van der Loos CM, et al. Site of intimal rupture or erosion of thrombosed coronary atherosclerotic plaques is characterized by an inflammatory process irrespective of the dominant plaque morphology. *Circulation*. 1994;89:36–44.
26. Townsend DW, Cherry SR. Combining anatomy and function: the path to true image fusion. *Eur Radiol*. 2001;11:1968–1974.
27. Klutz PG, Meltzer CC, Villemagne VL, et al. Combined PET/CT imaging in oncology: impact on patient management. *Clin Positron Imaging*. 2000;3:223–230.
28. Tawakol A, Elmaleh D, Fischman AJ, Muller J, Gewirtz H, Daghighian F. Intravascular characterization of atherosclerotic lesions with ¹⁸F-FDG and novel intravascular beta probe [abstract]. *J Nucl Med*. 2002;43(suppl):3P.
29. Mukai T, Nohara R, Kataoka K, Kanoi T, Konishi J, Saji H. Development and evaluation of a catheter-based radiation detector for endovascular detection of atheromatous plaques [abstract]. *J Nucl Med*. 2002;43(suppl):168P.





The Journal of
NUCLEAR MEDICINE

^{18}F -FDG Accumulation in Atherosclerotic Plaques: Immunohistochemical and PET Imaging Study

Mikako Ogawa, Seigo Ishino, Takahiro Mukai, Daigo Asano, Noboru Teramoto, Hiroshi Watabe, Nobuyuki Kudomi, Masashi Shiomi, Yasuhiro Magata, Hidehiro Iida and Hideo Saji

J Nucl Med. 2004;45:1245-1250.


This article and updated information are available at:
<http://jnm.snmjournals.org/content/45/7/1245>

Information about reproducing figures, tables, or other portions of this article can be found online at:
<http://jnm.snmjournals.org/site/misc/permission.xhtml>

Information about subscriptions to JNM can be found at:
<http://jnm.snmjournals.org/site/subscriptions/online.xhtml>

The Journal of Nuclear Medicine is published monthly.
SNMMI | Society of Nuclear Medicine and Molecular Imaging
1850 Samuel Morse Drive, Reston, VA 20190.
(Print ISSN: 0161-5505, Online ISSN: 2159-662X)

© Copyright 2004 SNMMI; all rights reserved.

 SOCIETY OF
NUCLEAR MEDICINE
AND MOLECULAR IMAGING